Rapid #: -22268270

CROSS REF ID: **5999069**

LENDER: **LQ0 (Queensland University of Technology) :: Main Library**

BORROWER: **LUU (Louisiana State University) :: Main Library**

TYPE:	Article CC:CCG
JOURNAL TITLE:	International journal of computer integrated manufacturing
USER JOURNAL TITLE:	International Journal of Computer Integrated Manufacturing
ARTICLE TITLE:	A robotic 3D printer for UV-curable thermosets: dimensionality prediction using a data-driven approach.
ARTICLE AUTHOR:	Velazquez, Luis,
VOLUME:	-
ISSUE:	
MONTH:	
YEAR:	2023
PAGES:	1-18
ISSN:	0951-192X
OCLC #:	

Processed by RapidX: 3/19/2024 10:43:32 PM

International Journal of Computer Integrated Manufacturing

ISSN: (Print) (Online) Journal homepage: www.tandfonline.com/journals/tcim20

A robotic 3D printer for UV-curable thermosets: dimensionality prediction using a data-driven approach

Luis Velazquez, Genevieve Palardy & Corina Barbalata

To cite this article: Luis Velazquez, Genevieve Palardy & Corina Barbalata (18 Sep 2023): A robotic 3D printer for UV-curable thermosets: dimensionality prediction using a data-driven approach, International Journal of Computer Integrated Manufacturing, DOI: 10.1080/0951192X.2023.2257652

To link to this article: https://doi.org/10.1080/0951192X.2023.2257652

INTERNATIONAL JOURNAL OF COMPUTER INTEGRATED MANUFACTURING
https://doi.org/10.1080/0951192X.2023.2257652

A robotic 3D printer for UV-curable thermosets: dimensionality prediction using a data-driven approach

Luis Velazquez, Genevieve Palardy and Corina Barbalata

Department of Mechanical and Industrial Engineering, Louisiana State University, Baton Rouge, LA, USA

ABSTRACT

This paper presents a robotic 3D printer specifically designed for ultraviolet (UV)-curable thermosets, whose printing parameters can be selected by using a predictive modeling strategy. A specialized extruder head was designed and integrated with a UR5e robotic arm. Software packages were developed to enable the communication between the extruder head and the robotic arm, and control systems were implemented to regulate the printing process. A predictive approach using either a feedforward neural network (FNN) or convolution neural network (CNN) is proposed for estimating the dimensions of future prints based on the process parameters. This enables selection of the appropriate parameters for high-quality prints. This strategy aims to decrease expensive trial-and-error campaigns for material and printing parameter tuning. Experimental results demonstrate the capabilities of the robotic 3D printer and the accuracy of the predictive approach.

ARTICLE HISTORY
Received 22 December 2022
Accepted 7 August 2023

KEYWORDS
UV-curable thermosets; robotic system; additive manufacturing; machine learning

1. Introduction

Automation for additive manufacturing (AM) technologies by means of robotics offers greater freedom of movement compared with conventional gantry designs, larger print volumes from system mobility around the printing space on wheels or rails, and reduced human supervision and interaction Tiryaki, Zhang, and Pham (2019a). These lead to a potential reduction in manufacturing cost, labor, and time, while providing an increase in productivity. Academia and industry have capitalized on these benefits to create commercially viable options for polymers and their composites, mostly focusing on thermoplastic 3D printing, including fiber-reinforced thermoplastics Urhal et al. (2019); Arevo (2022); Miri et al. (2022). AM of thermoset resins and their composites have gained research momentum in the past years because of their excellent thermal stability, specific strength and stiffness, and potential for multifunctionality and free-standing printing Li et al. (2019); Wu et al. (2019); Hershey et al. (2019); Gao, Qiu, and Wang (2022); Abedin et al. (2022a); Deng et al. (2023). Their use is however limited because curing behavior needs to be accurately controlled during deposition to enable high dimensional stability. To achieve such capabilities, one approach is to use ultraviolet (UV)-assisted curing for a photopolymer resin as it is extruded. However, to obtain a polymer viscosity suitable for AM extrusion, incorporating fillers or fibers may be required, which increases the complexity of using such materials with robotic systems. Nevertheless, success has been achieved with thermoset photopolymers and robotic manipulators to manufacture objects of various sizes, reinforced with continuous fibers Moi Composites (2022); Continuous Composites (2022). However, those systems and end-effector extruders are not readily commercially available at affordable costs, which this paper aims to address.

To be effective and to produce high accuracy results, robotic 3D printers require significant tuning strategies and trial-and-error campaigns, leading to expensive manufacturing processes. Predictive modeling and analysis is a promising approach to reduce development costs and to increase the applicability of robotic systems for AM with thermosets. Overviews of modeling approaches for AM were presented in the literature (Bikas, Stavropoulos, and Chryssolouris (2016); El Moumen, Tarfaoui, and Lafdi (2019), which summarized main research challenges based on

CONTACT Corina Barbalata cbarbalata@lsu.edu Department of Mechanical and Industrial Engineering, Louisiana State University, Patrick F. Taylor Hall, Baton Rouge, LA 3261, USA

manufacturing technologies. Dimensional accuracy modeling was seen as one of the main approaches to understand the outcomes of AM, including the importance of process parameters on part quality Westbeek et al. (2020).

Data-driven approaches, such as machine learning (ML), have had great success in modeling and analysis for both robotics Carlucho, Stephens, and Barbalata (2021); Costa et al. (2019) and material science Yan et al. (2021); Yan et al. (2021). In recent years, neural networks have been investigated for sample quality evaluation or layer dependencies, showing the capabilities of these approaches for predictive modeling when standard 3D printers are used Li et al. (2019); Banadaki et al. (2022). Learning from previous studies, this paper aims to advance the area of AM by proposing a data-driven predictive framework capable of estimating the dimensions of future 3D printed specimens when robotic manipulators and UV-curable thermosets are integrated, as seen in Figure 1. The proposed approach will enable users to select printing parameters and adjust material properties to improve print quality without expensive trial-and-error campaigns, reducing cost and material waste. Thus, this paper will make the following technical contributions:

- Design of a specialized end-effector for robotic systems using UV-curable thermosets in an AM process.
- Development of a data-driven predictive architecture to estimate dimensions of future 3D printed specimens, based on material characteristics and robotic parameters.

The structure of the paper is a follows: the literature review is presented in Section 2, followed by a description of the experimental setup in Section 3 and the predictive architecture in Section 4. These will be followed by conclusions and proposed future work in Section 5.

2. Background

This section provides an overview of main technologies used for additive manufacturing printing with thermosets, and introduces robotic systems and data-driven approaches integrated in AM.

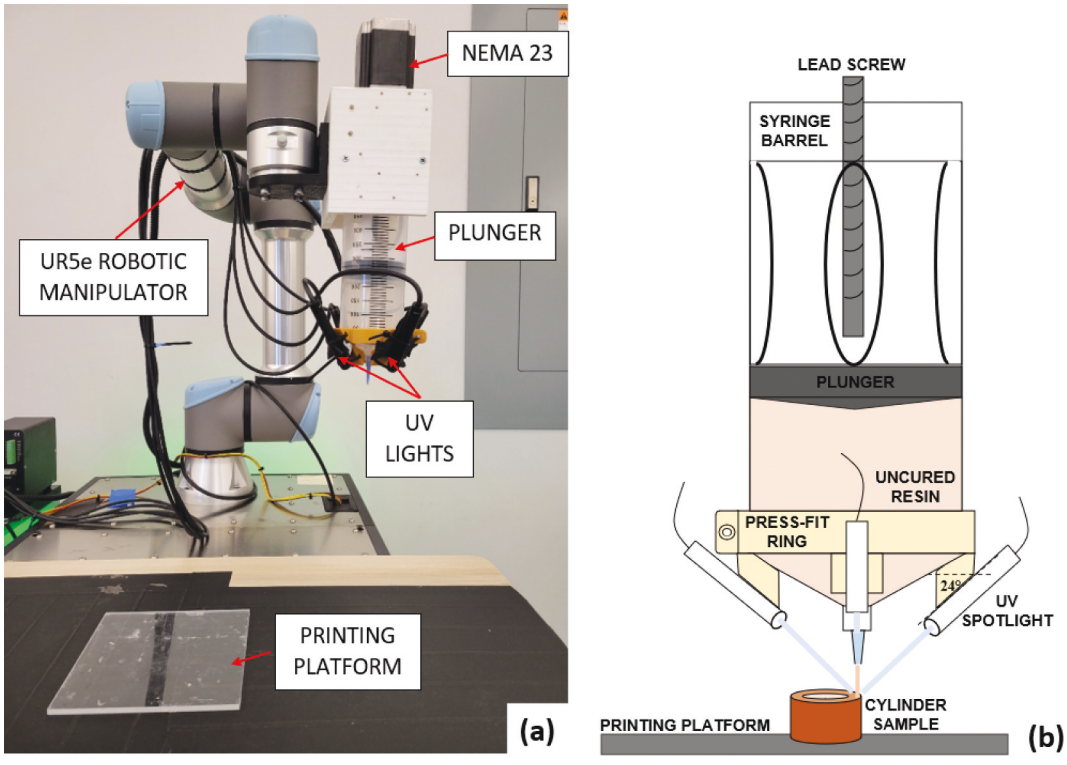

Figure 1. (a) robotic 3D printer with custom-designed end-effector, and (b) detailed schematic of end-effector.

2.1. Additive manufacturing technologies for thermosets

Current additive manufacturing technologies for thermosets typically use liquid resins (generally acrylic, epoxy, or vinyl ester) to manufacture parts through vat polymerization or extrusion-based techniques. The first category includes commercial processes such as Stereolithography (SLA) and Digital Light Processing (DLP), which rely on a UV light source or a digital micro-mirror device, respectively, to cure a part layer by layer. While they allow for high resolution, they are limited to planar configurations and confined to the resin vat Park et al. (2022). Extrusion-based processes encompass Direct Ink Writing (DIW), which has gained popularity in the past years for a range of feedstock materials Gao, Qiu, and Wang (2022); Romberg et al. (2021). It consists of either material extrusion or droplet deposition on a substrate and has been studied with a wide range of in-situ curing methods for thermosets (unreinforced or fiber-reinforced), including reaction curing, UV irradiation curing, temperature curing, or a combination of methods Gao, Qiu, and Wang (2022); Wang et al. (2020); Uitz et al. (2021); Wang et al. (2019); Ziaee, Johnson, and Yourdkhani (2022); Kopatz et al. (2021). UV curing, implemented with DIW, is a promising approach for free-standing printing of thermoset polymers. Its free-form capabilities were demonstrated with modified desktop printers or gantry systems Wu et al. (2019); Mizuno, Pardivala, and Tai (2018); Abedin et al. (2022b); Tu and Sodano (2021); Chen et al. (2018); Farahani et al. (2014) and custom-designed 5-axis systems Asif et al. (2018). The extruder head designs typically include micro-pumps, syringe pumps, or pneumatic regulators to deliver resin to the nozzle, and multiple laser diodes to cure resin as it is extruded. AM of continuous fiber-reinforced UV-curable thermosets has also been investigated through desktop systems equipped with a dispensing syringe fitted with a pneumatic regulator (Abdullah et al. 2023); He et al. (2021). In those studies, through extensive experiments, complex interactions between resin viscosity and formulation, nozzle geometry, and printing speed were observed and those parameters were important to control the quality of printed specimens.

2.2. Robotic additive manufacturing

The main advantage of robotics in AM is the realization of large-scale, complex 3D printed parts in relatively short periods of time. A complete overview of different robotic AM strategies using extrusion or direct metal deposition was given in Jiang, Newman, and Zhong (2021). Furthermore, a summary of polymers directly relevant for robotic applications was presented in Delda et al. (2021), highlighting their benefits in both industry and academia. A robotic manipulator for AM and its integration with deposition modeling techniques was described in Bin Ishak, Fisher, and Larochelle (2016) and further discussed in Luu and Hung Manh (2021), expanding on the extruder's control system and using polylactic acid (PLA). In the latter, an Arduino microcontroller was used to regulate the filament extrusion rate and the temperature at the nozzle. In Wu et al. (2017), a collaborative UR3 robot was utilized as a continuously moving printing platform with an Fused Deposition Modelling (FDM) extruder fixed on a frame, enabling printing of complex shapes and focusing on the fabrication sequence planning. Motion planning is one of the main areas of interest in the robotic 3D printing community. The design of an extrusion based end-effector was presented in Velazquez, Palardy, and Barbalata (2021), which can be integrated with robotic manipulators and UV-curable polymers. In Shembekar et al. (2019), an algorithm was developed to produce non-planar trajectories for AM robotic arms. Motion planning for mobile manipulators performing large-scale robotic AM using cement was presented in Tiryaki, Zhang, and Pham (2019b) and Zhang et al. (2018). While Tiryaki, Zhang, and Pham (2019b) focused on the coordination of the base, the manipulator, and the extruder deposition rate for a single robot, a multi-agent system was introduced in Zhang et al. (2018).

In industry, companies such as Continuous Composites, Inc. (USA) and Moi Composites (Italy), have demonstrated AM of continuous fiber-reinforced/UV-curable thermosets with robotic manipulators and custom-designed printing heads

Tyler (2014). However, they use continuous fiber-reinforced thermosets, a different type of material than our proposed work, for which no commercial end-effector is available. With this work, we aim to further expand the capabilities of robotic additive manufacturing by designing a specialized extruder head for UV-curable thermosets that can be integrated with collaborative robotic manipulators, such as the UR5e robotic system.

2.3. Data-driven approaches in additive manufacturing

Machine learning techniques were shown effective when applied to AM processes, given their good performance in pattern recognition and regression tasks. For example, they were used in image processing architectures to assess the quality of 3D printed thermoplastics . This may also enable real-time adjustment of printing parameters to address problems as they arise. A Neural Network (NN) was used as a pre-processing step in AM to predict part deformation due to residual stresses and create new geometries that would result in higher dimensional accuracy Nycz et al. (2021). A Long Short-Term Memory (LSTM) network was presented in Zhang, Wang, and Gao (2020) for the study of the dependencies between the layer-by-layer printing process and the final product quality. The FDM process was studied, considering the quality evaluation based on the tensile strength of the printed parts. A similar approach was discussed in Chen et al. (2021), where a generalized recurrence network was applied on the AM spatial image data to predict the behavior in each printed layer. Delli *et al*. leveraged support vector machine (SVM) to predict the quality of 3D printed samples with a conventional FDM printer Delli and Chang (2018). The model was used to classify the samples into"good" or"defective" categories using images gathered with an overhead camera. A CNN was developed in Garfo et al. (2020) for the automatic detection of surface defects in 3D printed concrete structures. In Xiong et al. (2014), a FNN was used to predict weld bead geometry, which showed promise as an effective approach to estimate the quality of printed specimens.

ML approaches were investigated for process planning as well, a crucial component of robotic additive manufacturing. Zohdi *et al*. used a genetic algorithm and gradient-based scheme to optimize the behavior of a robotic arm with a specialized extruder for additive manufacturing Zohdi (2018). A model-based reinforcement learning technique was presented in Dharmawan et al. (2020) to understand the effect of process parameters in multi-layer deposition in wire arc additive manufacturing (WAAM). Furthermore, the proposed approach corrected for inter-layer geometric digressions to ensure high accuracy prints. In Nicholas et al. (2020), a NN was used to enable a robotic arm to print onto unknown and arbitrarily shaped 3D substrates. In this case, a generative NN was leveraged to create the robotic arm path producing high accuracy samples.

There is significant potential for ML in AM since there are several technologies and opportunities on the manufacturing line where optimization, classification, and computer-vision tasks can be incorporated. As presented above through a literature review, the primary focus is on quality assessment using regular printing capabilities, or process and motion planning for robotic 3D printers. This work aims to close the gap between the two areas and leverage ML approaches to predict the quality of future printed specimens when robotic manipulators are used in the process. This novel approach would decrease the prototyping time and reduce expensive trial-and-error campaigns when material properties are modified and/or new setups are used.

3. Experimental setup: materials and custom extrusion head

This section presents the design and implementation of a new experimental setup to advance the capabilities of robotic AM technology utilizing extrusion of UV-curable thermosets. The materials used for robotic additive manufacturing and their rheological characterization are first presented, followed by a description of the custom-based extrusion system and its integration with the robotic manipulator. The overall robotic additive manufacturing technology with the mounted extrusion system is shown in Figure 1. Lastly, examples of 3D printed specimens with the proposed system are presented in this section.

3.1. Thermoset material and rheological characterization

The thermoset resin used in this study is a commercially-available acrylic-based photopolymer (purchased from Anycubic). It is typically used for SLA and DLP printing, and it was shown to polymerize under UV exposure during DIW Mizuno, Pardivala, and Tai (2018); Velazquez, Palardy, and Barbalata (2021); Weger et al. (2022). It has an UV wavelength between 365 nm and 410 nm, with a viscosity at room temperature (25°C) ranging from 150 to 200 mPa.s. As viscosity was expected to influence the printed specimens' dimensional stability, fumed silica (FS, AEROSIL R972, from VWR), a common filler to modify viscosity of polymers, was incorporated at three weight fractions: 2.8%, 6.0%, and 8.0% Romberg et al. (2021); Tu and Sodano (2021); Velazquez, Palardy, and Barbalata (2021); Asif et al. (2019).

A parallel plate Discovery Hybrid Rheometer 20 (DHR-20, Waters TA Instruments) was employed to measure shear viscosity for different resin formulations (0, 2.8, 6.0, and 8.0 with % FS). Resin samples were tested at 25°C with 25 mm diameter parallel plates in shear rate sweep mode from 0.1 to 100 s^{-1}. This data was used to assess the shear thinning behavior of the photopolymer.

A power fit was performed on the viscosity data to find a function that could predict the viscosity for the actual shear rate found at the extrusion nozzle with the given extrusion rate. This function was leveraged to generate specific viscosity values for each extrusion rate. Equation (1) shows the general relationship between viscosity, η (Pa.s), and shear rate, $\dot{\gamma}$ (s^{-1}):

$$\eta = a\dot{\gamma}^{b} + c \tag{1}$$

where the terms a, b, and c were found for each resin formulation through a power fit. To calculate $\dot{\gamma}$, standard fluid dynamics principles of shear rate in pipe flow were used. The main assumption was to treat the nozzle geometry as an approximation of a small diameter pipe. Equation (2) shows the general form for maximum shear rate in a pipe White (2011):

$$\dot{\gamma} = \frac{4Q}{\pi r_n^3} \tag{2}$$

where Q is the volumetric flow rate (m^3/s) and r_n is the nozzle radius (mm). Equation (2) can be further simplified as Equation (3), according to the geometry and specifications of the extrusion head:

$$\dot{\gamma} = \frac{L_t}{m r_n t_m} \tag{3}$$

where L_T (mm/rev) and t_m (ms) refer to the linear travel of the extruding plunger per revolution of the shaft and the half-time for one step of the motor, respectively. The magnitude per revolution, $m = 200$, is the result of simplifications in Equation (2).

3.2. End-effector design and integration with robotic manipulator

As there is no commercially-available extruder system for UV-curable thermosets integrated with robotic manipulators, the following paragraphs present the design of a specialized extruder head compatible with a UR5e manipulator. The end-effector was designed to allow for cost-effective and controllable extrusion rate of the photopolymer.

As seen in Figures 1 and 2, the extrusion system was installed on a UR5e robotic manipulator. It included a syringe capable of holding up to 200 mL of uncured thermoset resin. The syringe had an interchangeable nozzle through which material was extruded and deposited on a printing platform. The inner plunger in the barrel slid on a lead screw driven by a NEMA23 stepper motor at a predefined revolutions- per-minute (RPM), creating enough internal pressure to achieve extrusion rates up to approximately 5.3 mm^3/s. The stepper motor provided a torque of 1.9 Nm, sufficient to overcome internal friction and to extrude viscous resins. Several components of the extrusion system were 3D printed with PLA, including the L-shape connector that serves as attachment for the end-effector to the robotic arm, the housing of the syringe, the plunger, and the press-fit ring to mount the UV spotlights. For the purpose of this project, the choice of PLA instead of higher-strength materials (e.g. aluminum, acrylonitrile butadiene styrene (ABS)) offered cost-efficiency, as well as rapid and convenient modifications to the design during the prototyping phase.

The stepper motor ensured a controllable deposition rate. To achieve the desired extrusion rates, an Arduino UNO and a DM556T stepper driver were used to set the motor RPM and the rotation direction.

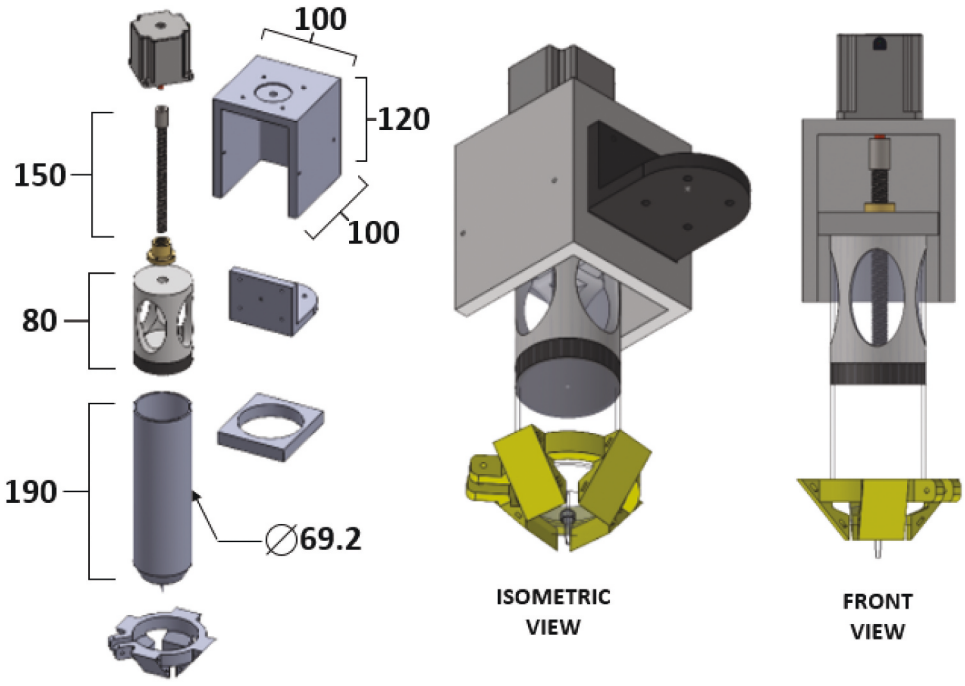

Figure 2. SolidWorks models of the assembled extruder and its main components. All dimensions are in mm.

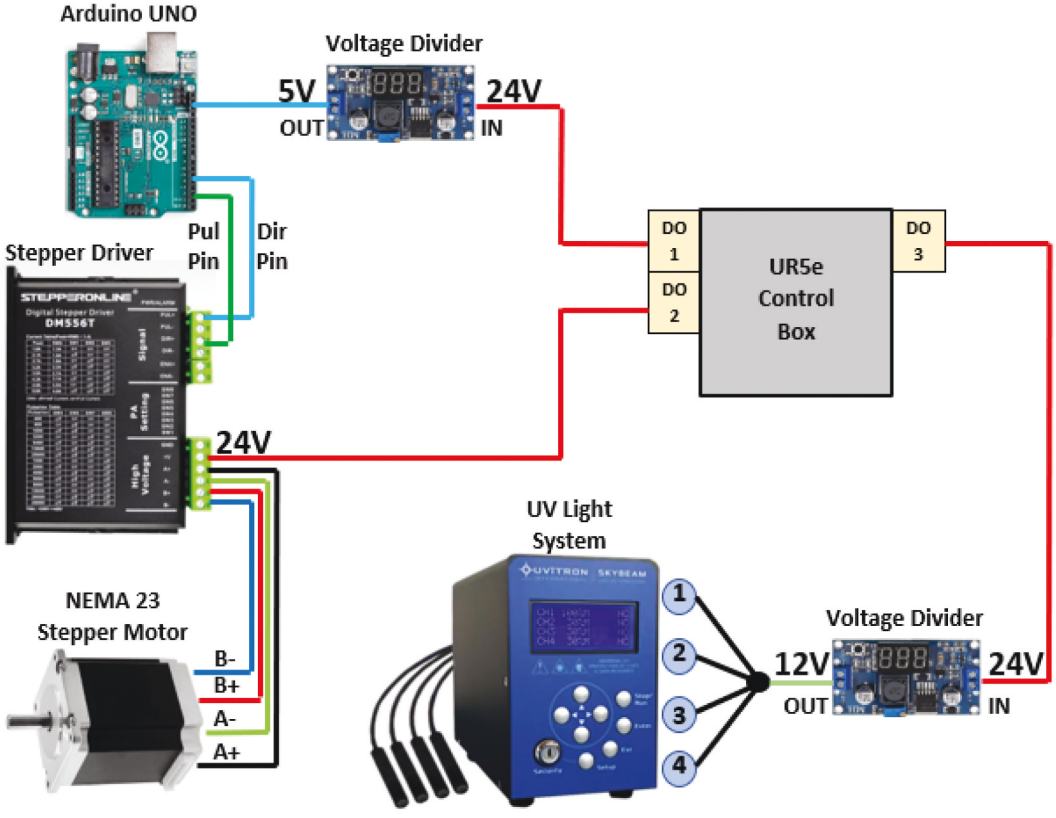

Figure 3. Electronic components of the extrusion system and its electrical connection to the robotic arm.

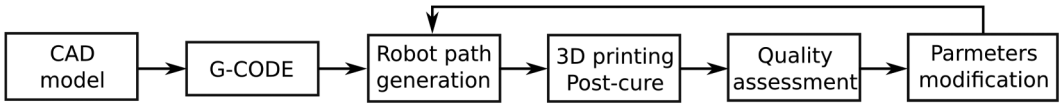

Figure 4. Additive manufacturing process flowchart using a UR5e robotic manipulator.

Figure 3 shows how the components of the robotic 3D printer communicate with each other and their integration with the robotic manipulator. The stepper motor was connected to the driver, further connected to the Arduino UNO. Two Digital Output (DO) signals from the robotic controller turned the Arduino board and stepper motor on and off.

The extruded material was exposed to four SkyBeam UV spotlights (10 W, 365 nm wavelength, UVitron International) to achieve partial curing of the printed specimens. The UV light system had four channels, each connected to a 6 mm lens spotlight, attached to the syringe through a press-fit ring. Irradiance on the extruded material reached 5.6 W/cm^2 at a distance of 13 mm, however, only 1% of the total power was used to 3D print the specimens, based on previous work Velazquez, Palardy, and Barbalata (2021). The spotlights angle was 24 degrees from all four directions to cover the area where material was extruded. A DO signal from the robotic arm control box directed the lights to turn on and off as needed during the extrusion process. In addition, voltage dividers ensured that proper voltage was delivered to each electronic component in the system since the control box output was 24 V.

The flowchart in Figure 4 is a summary of the steps to 3D print the designed specimens. The process started with a computer aided design (CAD) model of the specimen. It was then sliced using Slic3r Slic3r (2022), a program with a high degree of customization for printing parameters, such as velocity, layer height, and nozzle diameter. Slic3r output the G-code with the coordinates and parameter values of the end-effector per individual layer.Figure 5(a) shows a rendering of the Slic3r environment where the samples were sliced and Figure 5(b) is an example of the RoboDK simulation environment used to generate the robot path while avoiding collision with the environment. Furthermore, RoboDK was also used to validate the printing behavior for the robot. The manufactured samples and their characterization are detailed in the following paragraphs.

3.3. Additively manufactured specimens

To first evaluate the performance of the robotic additive manufacturing technology, specimens were printed with the proposed system using the UV-curable acrylic-based thermoset described in Section 3.1. A summary of initial parameters and

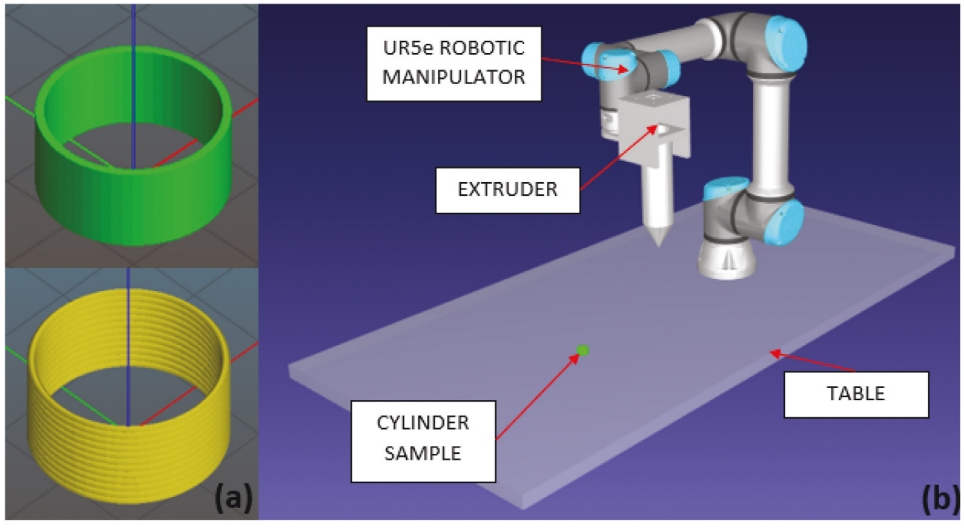

Figure 5. (a) Slic3r software environment for designed specimen, and (b) RoboDK simulation environment to validate robotic printing paths.

Table 1. Experimental parameters for initial 3D printed specimens with the robotic system. FS: fumed silica.

Parameter	Level 1	Level 2	Level 3
FS weight fraction [wt%]	2.8	6.0	8.0
End-effector velocity [mm/s]	4	7	10
RPM delay [ms]	2000	2500	3000
Layer height [mm]	0.5	1.1	1.2

their levels is provided in Table 1, including FS weight fraction, robot end-effector velocity, motor RPM delay, and layer height. The nozzle diameter and UV light power were fixed for all experiments as 2 mm and 1% of total power, respectively. After printing, all specimens were post-cured in an Intelliray 600 chamber (UVitron International) for 60 seconds at 85% intensity to achieve full cure.

Various geometries were printed to demonstrate the capabilities of the proposed robotic system. Figure 6(a-c) show cylindrical, pyramidal, and conical samples during the printing process, while Figure 6 (d-e) present different shapes manufactured with the robotic system. A cylindrical geometry, as seen in Figure 5(a), was selected for future experiments to develop the predictive approach. Cylindrical specimens were chosen due to their feasibility to be characterized with only three dimensions (outer diameter, height, and wall width), facilitating dimensional accuracy analysis.

Figure 7 shows representative cylindrical specimens for different material and printing parameters listed in Table 1. In general, it was observed that viscosity, motor delay, and end-effector velocity most noticeably influenced the quality of the prints. In addition, notable interactions between those parameters were observed, as well as with layer height and nozzle geometry, the latter influencing the shear rate and viscosity at the nozzle exit, as shown in Equations (1) and (3). Overall, during the printing experiments, given the complex interactions between all parameters and material characteristics, extensive fine-tuning of printing parameters was required to achieve high-quality prints.

The nominal dimensions of the cylinder CAD model, as shown in Figure 5(a), were the following: outer diameter (OD) of 20 mm, height (H) of 12 mm, and wall width (WW) of 1.5 mm. For each printed cylinder, the dimensions were measured with a digital caliper. For each dimension, four measurements were taken and averaged per printed specimen. For example, the average dimensions for

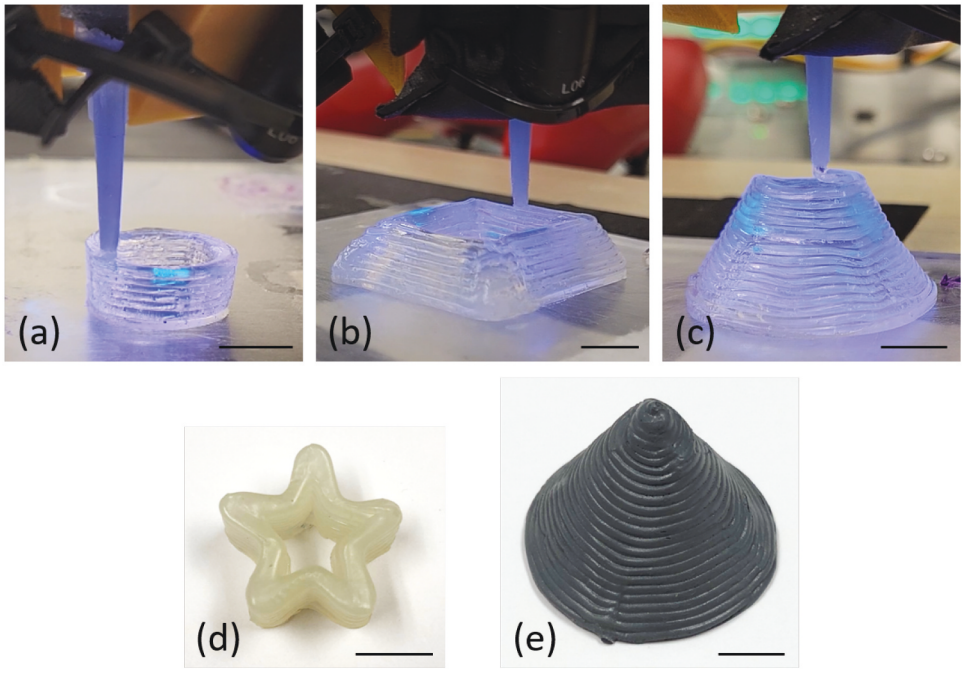

Figure 6. Additive manufacturing of various geometries: (a) cylinder, (b) pyramid, and (c) cone. Different 3D printed shapes with the robotic system: (d) star and (e) cone. The nozzle diameter and UV light power were fixed for all experiments as 2 mm and 1% of total power, respectively. Scale bars in (a)-(e): 10 mm.

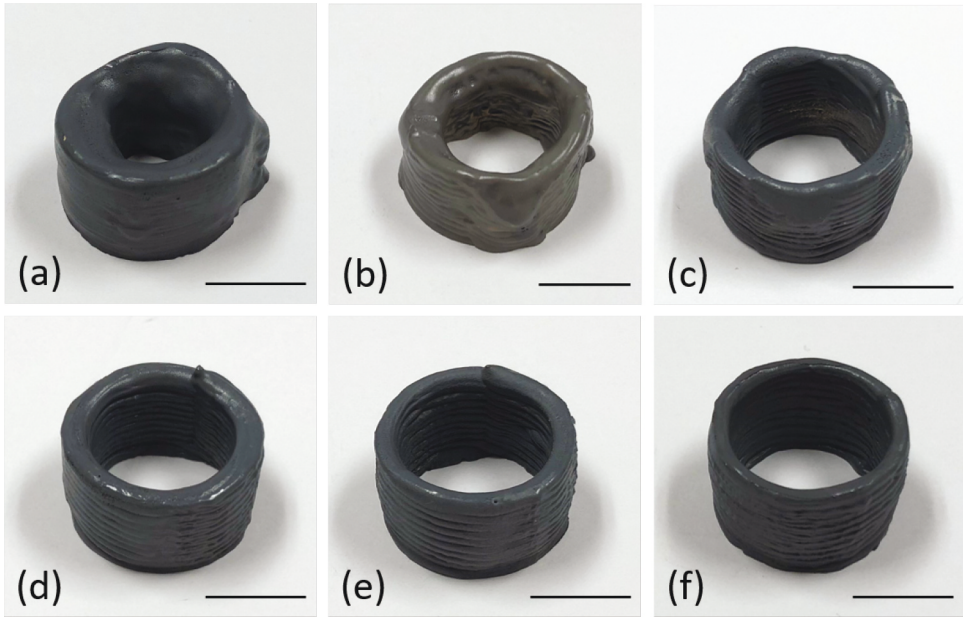

Figure 7. Cylindrical specimens manufactured with different material and printing parameters: (a) 2.8 wt% FS, 10 mm/s velocity, 2500 ms RPM delay, and 0.5 mm layer height, (b) 6 wt% FS, 4 mm/s velocity, 2500 ms RPM delay, and 1.1 mm layer height, (c) 8 wt% FS, 4 mm/s velocity, 2500 ms RPM delay, and 1.1 mm layer height, (d) 8 wt% FS, 4 mm/s velocity, 2000 ms RPM delay, and 1.2 mm layer height, (e) 8 wt% FS, 5 mm/s velocity, 2000 ms RPM delay, and 1.2 mm layer height, and (f) 8 wt% FS, 7 mm/s velocity, 2000 ms RPM delay, and 1.2 mm layer height. The nozzle diameter and UV light power were fixed for all experiments as 2 mm and 1% of total power, respectively. Scale bars in (a)-(f): 10 mm.

specimens in Figure 7(d-f) are the following: (d) OD = 23.22 $\pm$ 0.40 mm, H = 12.75 $\pm$ 0.39 mm, and WW = 3.62 $\pm$ 0.10 mm, (e) OD = 22.77 $\pm$ 0.26 mm, H = 12.64 $\pm$ 0.04 mm, and WW = 2.84 $\pm$ 0.11 mm, and (f) OD = 21.46 $\pm$ 0.23 mm, H = 12.42 $\pm$ 0.20 mm, and WW = 2.15 $\pm$ 0.05 mm.

4. Predictive dimensional accuracy estimation

The cylindrical specimens were used to better understand the connections between the parameters of the process. Specifically, these specimens were leveraged to predict the dimensional accuracy of future prints, when either robotic parameters or material properties are modified. The focus of this section is to demonstrate the applicability of supervised machine learning approaches, such as feedforward neural network (FNN) and convolution neural network (CNN), for this problem.

Figure 8 presents the data-driven predictive pipeline proposed in this work. Training data was collected from samples printed with the robotic system described in Section 3. The robotic and material parameters were configured before the printing process began, while the set of dimensional parameters characterizing each sample was extracted after full cure, detailed in the previous section. The predictive model

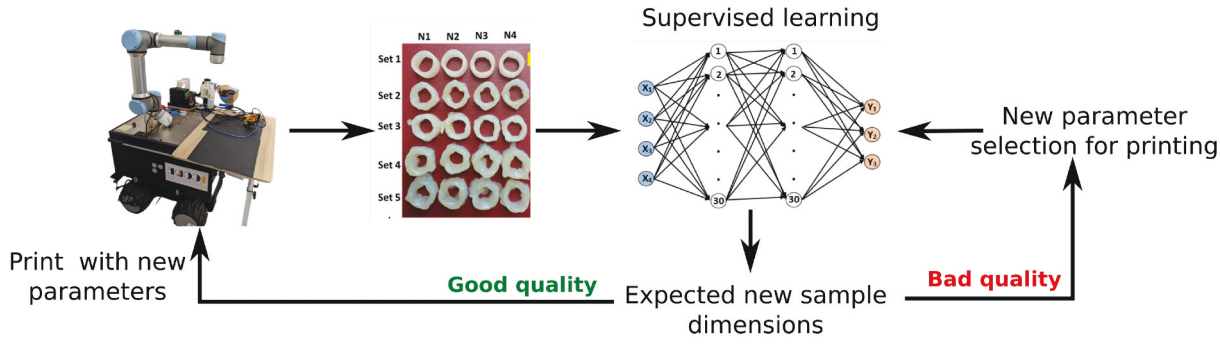

Figure 8. Overview of the proposed system for quality evaluation.

was then used to estimate the dimensions of future prints without the need to experimentally test the material-robot coordination and parameter selection. To validate the proposed approach, several material-robotic parameter combinations were used and the predicted dimensions were compared to the dimensions of the actual specimens printed with the robotic system under the same input conditions. In practice, it would mean that if the predicted quality of the print is considered acceptable, the actual 3D print can take place, but if the quality is unacceptable, different material-robotic parameters are selected and the process is repeated. In the following paragraphs, the two predictive models considered are described and the results of the predictive approach are analyzed.

4.1. Feedforward neural networks

As presented in Mitchell (1997), FNNs can map highly non-linear data and create a target function resilient to errors or noise. As such, FNNs is appropriate for estimating dimensional accuracy of 3D prints using UV curable thermosets, as acrylic-based photopolymers tend to deform as they undergo curing, introducing dimensional noise in the dataset.

Figure 9 shows the architecture of the FNN used to predict the dimensions of the 3D printed specimens. The proposed FNN had a total of four layers: one input, two hidden, and one output. The two hidden layers had 30 neurons each. The input variables were the motor RPMs, layer height, end-effector velocity, and resin viscosity. The latter was controlled by the FS weight fraction and nozzle geometry, as calculated from Equations (1)-(3) in Section 3.1. The outputs of the network were the dimensions measured from the cured printed specimens: height, wall width, and outside diameter.

For this application, back-propagation was used to update the weights. The loss function was based on the mean-squared error (MSE), as seen in Equation (4):

$$L = \frac{1}{N}\sum_{i=1}^{N}(x_i - y_i)^2 \tag{4}$$

where N represents the total number of data points, x_i is the returned model prediction, and y_i is the measured value of the i-th sample. This loss function computed the output error of the network, describing how close the predicted values were to the targets of the problem.

4.1.1. Training procedure

The strategy to collect the data consisted of varying one of the input variables within a range while keeping the other three constant. For each parameter combination, a cylinder was printed, post-cured, and its dimensions (outputs) measured with a digital caliper. A total of 187 specimens were obtained and for each dimension, measurements at four locations were taken and averaged. Table 2 summarizes the input variable ranges that were investigated. As previously

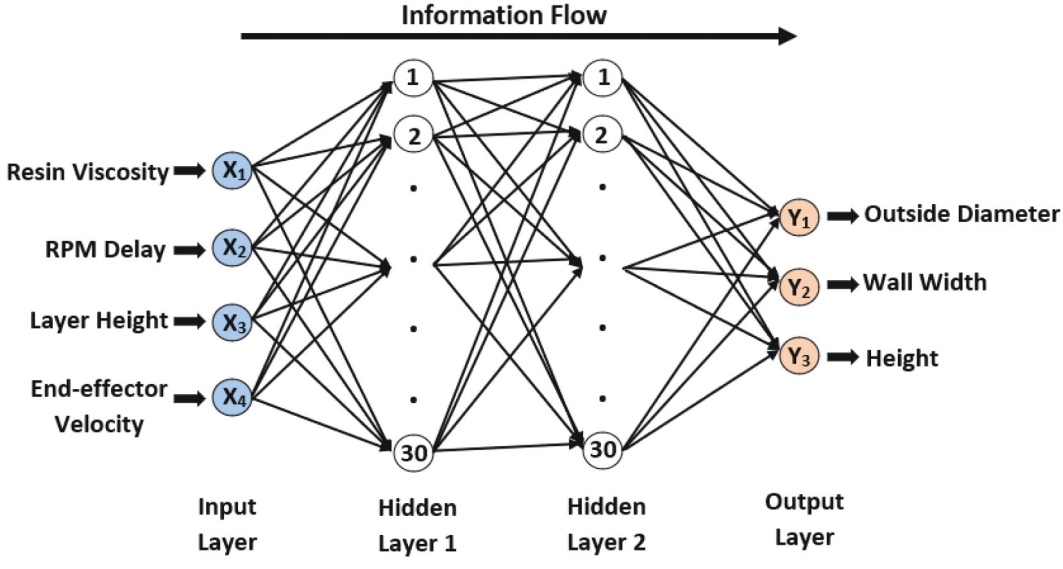

Figure 9. Architecture of the proposed FNN with two hidden layers.

Table 2. Input variable ranges for a three-layer FNN.

Input Variable	Range
Resin viscosity at nozzle [Pa.s]	1.5 – 70.0
RPM delay [ms]	900 – 3800
Layer height [mm]	0.25 – 1.20
End-effector velocity [mm/s]	2.0 – 13.5

mentioned, the resin viscosity range was estimated from the procedure described in Section 3.1, using the nozzle geometry (1.5 mm or 2 mm diameter) and power fit over the rheological data.

Random testing sets were selected out of the total number of samples, containing approximately 20% of the total number of data points, or 37 samples. The rest of the data set (150 data points) was used for training. The $80\% - 20\%$ ratio between training and testing samples was shown to be appropriate for generating the best results, avoiding over-fitting Gholamy, Kreinovich, and Kosheleva (2018). Out of all the samples used for training, 30% were used for validation, following the same principle highlighted above. Furthermore, to guarantee that over-fitting was prevented, data augmentation was performed by adding Gaussian noise to the input data, creating a new training data set consisting of 300 samples. This approach ensured that the learned features were robust and also enhanced the generalization capability of the model.

4.1.2. Testing results

To evaluate the performance of the architecture, the testing set was used to predict the printed cylinder height, wall width, and outside diameter. These were then compared with the measured dimensions of the real printed specimens to evaluate the success of the approach. Training and testing took place on an Intel(R) Core(TM) $i7 - 9750H$ CPU @2.60GHz. As the data set available had a limited number of samples, training and testing procedures were repeated multiple times, by randomly selecting the testing set and using the remainder of the samples for training, leading to 10 training-testing scenarios.

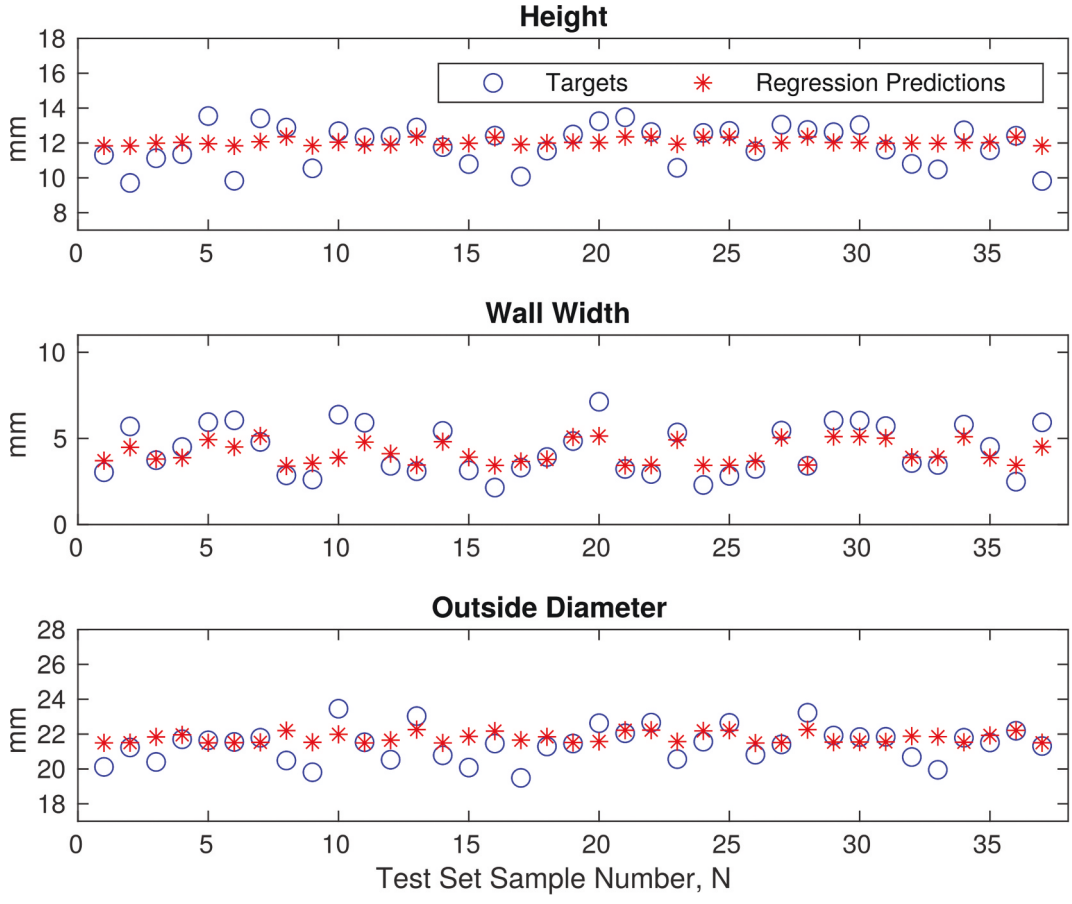

Figure 10. Comparison between the FNN cylinder dimensions prediction ("NN predictions") and the actual cylinder values ("Targets").

Table 3. Minimum and maximum errors with standard deviation for dimensions prediction with the FNN approach.

	Height	Wall Width	Outside Diameter
Minimum absolute error [mm]	0.003	0.015	0.008
Maximum absolute error [mm]	2.03	1.38	2.79
Standard deviation [mm]	0.30	0.33	0.40

Table 4. RMSE for each dimension estimation when FNN is used with data augmentation.

Test #	Height RMSE [mm]	Width RMSE [mm]	Diameter RMSE [mm]
1	0.43	0.16	0.12
2	0.27	0.20	0.12
3	0.33	0.40	0.52
4	0.35	0.20	0.25
5	0.33	0.47	0.24
6	0.27	0.53	0.29
7	0.42	0.30	0.25
8	0.43	0.30	0.13
9	0.35	0.32	0.36
10	0.26	0.22	0.25

Table 5. Minimum and maximum errors with standard deviation for dimensions prediction using data augmentation with the FNN implementation.

	Height	Wall Width	Outside Diameter
Minimum absolute error [mm]	0.07	0.11	0.01
Maximum absolute error [mm]	4.33	4.58	5.04
Standard deviation [mm]	0.42	0.54	0.55

In the case with no data augmentation, the average Root-Mean-Square Error (RMSE) for the FNN configuration was 0.24 mm over 10 training-testing scenarios, with an average time of 10 seconds during training. This average includes the RMSE values of the height, wall width, and outside diameter for the FNN predictions, when compared to the actual targets from the testing set. An example of the results is shown in Figure 10, where it is observed that the predicted dimensions for almost all samples are in close proximity to those measured on the real samples. During these 10 training-testing runs, the minimum and maximum absolute errors were computed together with the standard deviation, as presented in Table 3. These results show the variability in the predicted dimensions with some samples closely estimated, while others displayed errors over 2 mm for one dimension.

4.1.2.1. Data augmentation. With data augmentation, the RMSE for the predicted height, width, and outside diameter values are shown in Table 4 for 10 different training-testing runs. For each test, the training set consisted of 300 samples while the testing set had 37 randomly selected samples. Similar results were observed over all tests with comparable RMSE for all dimensions considered. Based on the minimum and maximum absolute errors and the standard deviation summarized in Table 5, the highest and smallest variability were both obtained for the outside diameter.

4.2. Cascade neural networks

To further demonstrate the capabilities of predictive parameter selection, a CNN that moves the information forward, while each layer is connected to every subsequent layer of the network, was also considered. These additional connections in the CNN could improve the data distribution over the network and reveal more information about the nature of the relationship between the inputs and outputs of the model Alkhasawneh and Tien Tay (2018); Mohammadi et al. (2021). The proposed CNN had an identical architecture to the proposed FNN, with the exception of the added links between the layers. The chosen architecture is illustrated in Figure 11, where the inputs and outputs of the network are similar to the ones used in the FNN approach.

4.2.1. Training procedure

An identical procedure to the FNN was followed to evaluate the performance of the CNN in terms of predictions made on randomly selected test sets of the same data, consisting of 187 specimens, out of which 37 were used for testing. Two hidden layers, each with 30 neurons, were used. The loss function was defined in Equation (4), using a tan-sigmoid as the transfer function for the hidden layers. Weights and bias were updated according to a Levenberg-Marquardt optimization. Similarly to the FNN approach, data augmentation was also investigated using Gaussian noise, increasing the number of training samples to 300.

4.2.2. Testing results

The proposed CNN configuration proved to be as accurate as the FNN to predict the geometrical dimensions of the samples. The average RMSE obtained after 10 training-testing scenarios (no data augmentation) was 0.108 with an average training time of 8 seconds. An example of one of those tests is presented in Figure 12. In Table 6, the minimum and

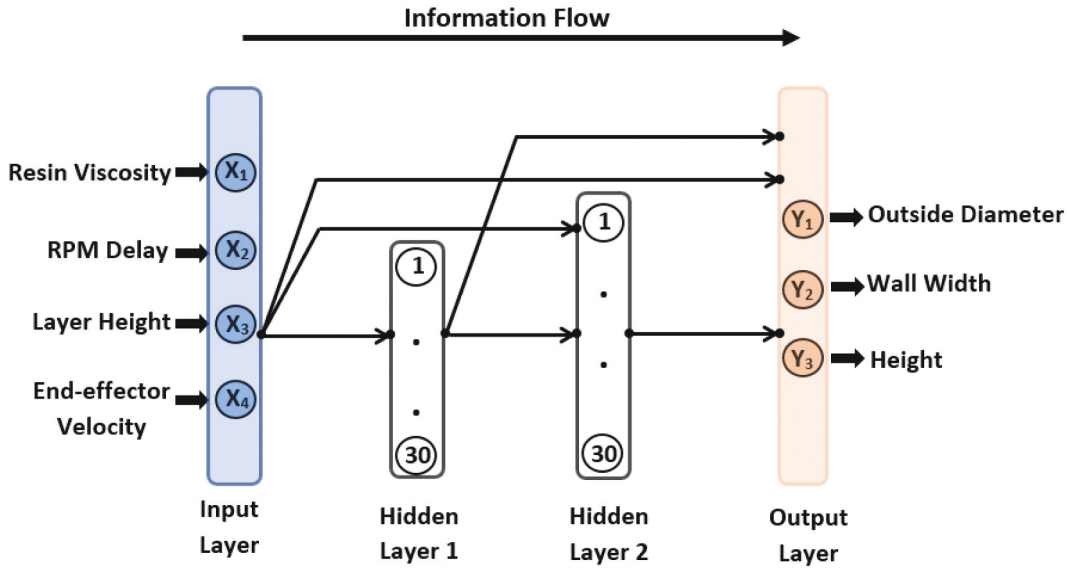

Figure 11. Architecture of the proposed CNN with two hidden layers and 30 neurons in each layer.

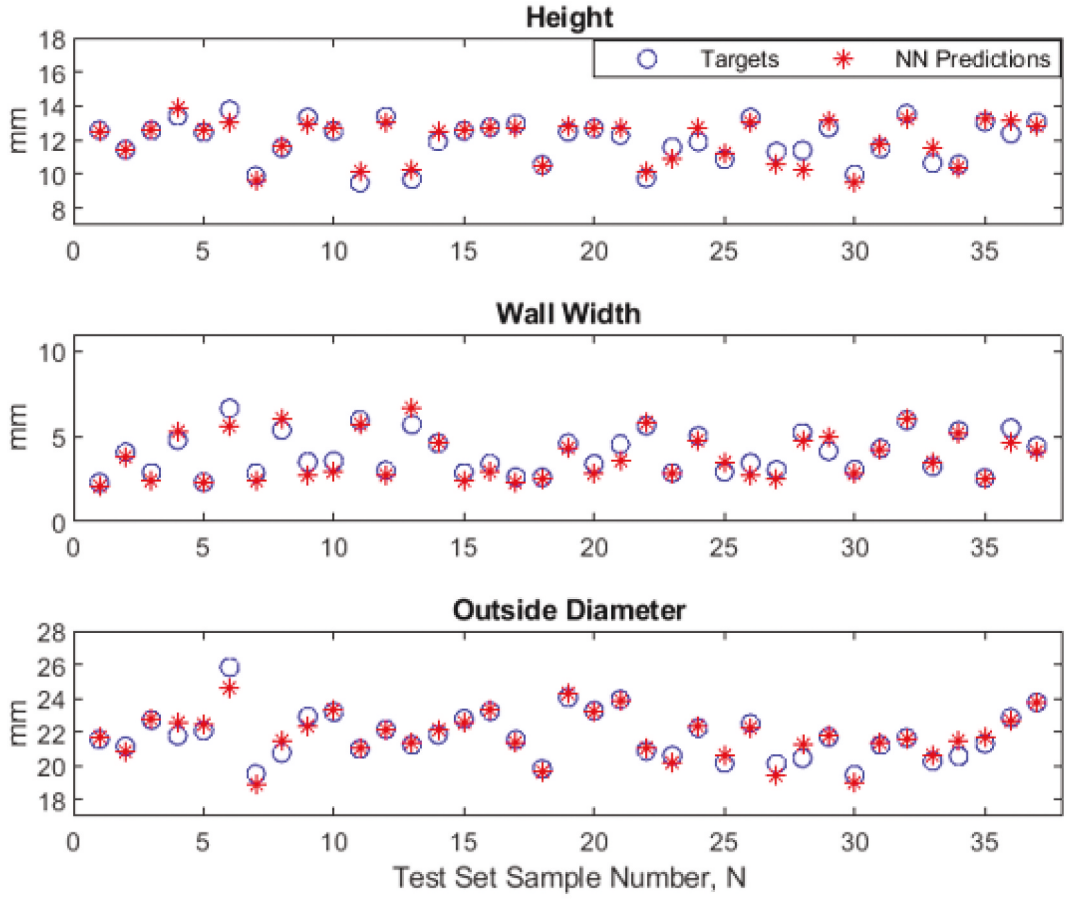

Figure 12. Comparison between the CNN cylinder dimension predictions ("NN predictions") and the actual 3D printed cylinder values ("Targets").

Table 6. Minimum and maximum errors with standard deviation for dimensions prediction with the CNN approach.

	Height	Wall Width	Outside Diameter
Minimum absolute error [mm]	0.01	0.03	0.007
Maximum absolute error [mm]	1.00	2.49	1.73
Standard deviation [mm]	0.24	0.35	0.34

Table 7. Minimum and maximum errors with standard deviation for dimensions prediction using data augmentation with the CNN implementation.

	Height	Wall Width	Outside Diameter
Minimum absolute error [mm]	0.002	0.01	0.04
Maximum absolute error [mm]	5.15	3.09	2.31
Standard deviation [mm]	1.04	0.56	0.55

maximum absolute errors were computed with the standard deviation for the 10 training-testing scenarios. In this case, there are smaller deviations among tests, compared to the FNN approach.

4.2.2.1. *Data augmentation.*

With data augmentation, the minimum and maximum absolute errors are shown in Table 7 over the 10 training-testing scenarios, where the testing data set was randomly selected for each run. The estimated deviations for the wall width and outside diameter were consistent among each other, while a larger deviation was obtained for the samples' height. These results are generally consistent with the case when no data augmentation was used.

4.3. *Discussion*

Before employing the FNN and CNN approaches for estimating the dimensions of future 3D prints, regression analysis was considered. Nevertheless, due to the multi-dimensional formulation of the problem and no linear correlations between the features and target outputs, this approach did not produce good accuracy, even on the training data. An example of the outputs of the linear regression is shown in Figure 13, where the predictions result in an average of the actual target measures, for all three dimensions considered.

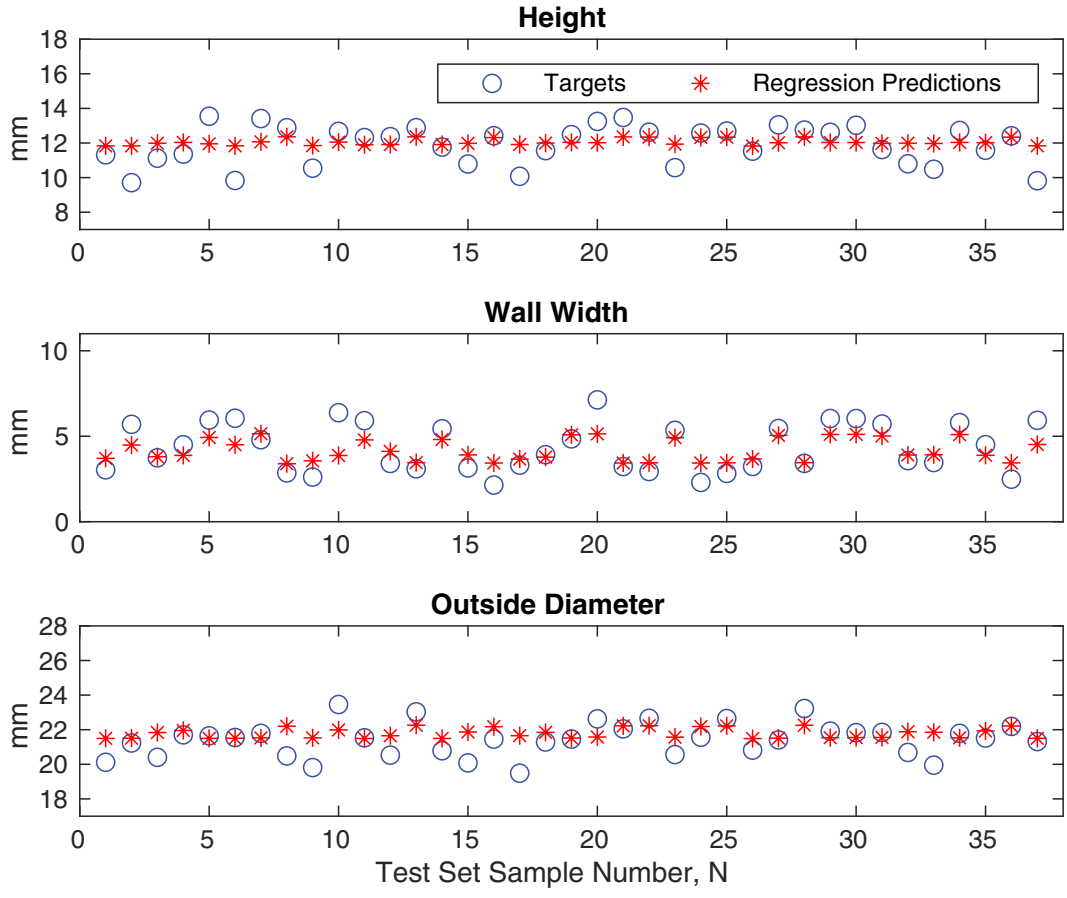

Figure 13. Comparison between regression predictions ("Regression predictions") and the actual 3D printed cylinder dimensions ("Targets").

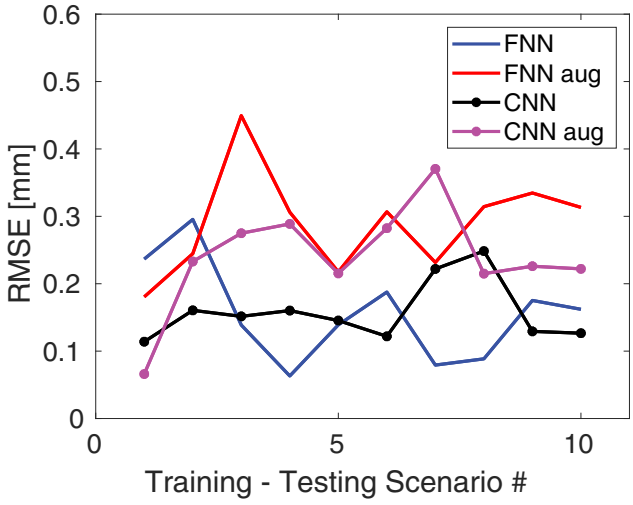

Figure 14. Comparison between RMSE for different network configurations of the proposed predictive estimation.

Although the data set was relatively small, machine learning approaches such as FNN and CNN architectures, were beneficial to approximate the dimensions of future prints, as shown in Figures 10 and 12. Two different networks were tested to demonstrate the feasibility of predictive dimension analyses, given limited experimental data sets. To address concerns regarding the small data sets and overfitting, data augmentation was performed. The results with and without data augmentation showed similar trends and successful estimation of the dimensions of 3D printed specimens when the input parameters were altered. The maximum error of 5.15 mm (Table 7) was obtained for the height of a sample for which the target was 18 mm. The average RMSE for each training-testing scenario and all network configurations is presented in Figure 14. All experiments returned an RMSE well under 1 mm, confirming that both FNN and CNN configurations are feasible.

The training sample size is important for any neural network predictive approach, as increasing the number of samples and their ranges can improve the performance of the model. Training was performed with 150 and 93 samples, for both the FNN and CNN approaches. When using the CNN to predict samples' dimensions, maximum prediction errors of 5.05 mm and 9.08 mm were obtained for the height when 150 and 93 samples were used, respectively. For the FNN approach, the maximum errors were 2.03 mm and 3.05 mm for the height when 150 and 93 samples were used, respectively. Nevertheless, if a large training set with similar characteristics is employed, the performance of the system can decrease due to overfitting, as was observed from Tables 7 and 4, where the maximum errors for the height of the samples increases compared to the case when no data augmentation was used. The proposed approach, working with a limited number of samples for training indicates that predictive models for 3D printed specimen dimensions can successfully help reduce the time spent manually tuning process parameters and the cost due to material waste. As novel materials are discovered, especially in the field of AM, such models are valuable to identify suitable process parameters and material characteristics leading to high-quality prints, reducing costs incurred by extensive experimental campaigns.

5. Conclusions

This paper introduced the design of a robotic additive manufacturing system capable of utilizing UV-curable thermosets. The system was used to additively manufacture various specimens and data-driven approaches were leveraged to predict printed samples' dimensions. The following conclusions and recommendations can be formulated:

- A custom-designed extruder head was integrated with a UR5e collaborative manipulator. Cylindrical, pyramidal, and conical samples with heights in the range of $10 - 20$ mm, and outside diameters or widths of $20 - 35$ mm were produced. As complex interactions were observed between printing parameters, material characteristics (i.e. viscosity), and printed specimens' quality, there was a need to create a data-driven predictive architecture to estimate dimensions of future AM specimens.
- Machine learning approaches were leveraged, such as feedforward neural network (FNN) and convolution neural network (CNN), to demonstrate their capabilities for predictive modeling. The proposed methods used the material and processing parameters as inputs, and the future 3D print dimensions as outputs, showing how the inputs affected dimensional accuracy. The

data set consisted of 150 cylindrical samples for training and 37 samples for testing. All predictions had an RMSE under 1 mm. Data augmentation was also considered resulting in 300 samples for the training dataset, and the results from both networks showed similar performance to the case without data augmentation. Overall, the proposed neural networks can be used to identify suitable robotic AM process parameters without extensive trial-and-error tuning campaigns.

In the future, larger experimental data sets will be created, with more complex geometries to further validate the proposed data-driven architecture, giving special attention to overhanging structures. In addition, more advanced predictive methods will be designed to increase the accuracy of the predictions. Finally, the extruder end-effector will be modified to allow continuous fiber-reinforced materials in the printing process.

Disclosure statement

No potential conflict of interest was reported by the author(s).

Funding

This work was supported by the Louisiana Board of Regents [LEQSF-EPS(2022)-LAMDASeed-Track1B-11]; Louisiana Board of Regents [LEQSF-EPS(2021)-LAMDASeed-Track1B-01]; Office of Integrative Activities [OIA1946231].

References

Abdullah, A. M., Y. Ding, X. He, M. Dunn, and Y. Kai. (2023) "Direct-Write 3D Printing of UV-Curable Composites with Continuous Carbon Fiber." *Journal of Composite Materials* 0 (0): 00219983221127182. https://doi.org/10.1177/00219983221127182.

Abedin, R., X. Feng, J. Pojman, S. Ibekwe, P. Mensah, I. Warner, and L. Guoqiang. 2022. "A Thermoset Shape Memory Polymer-Based Syntactic Foam with Flame Retardancy and 3D Printability." *ACS Applied Polymer Materials* 4 (2): 1183–1195. https://doi.org/10.1021/acsapm.1c01596.

Abedin, R., F. Xiaming, P. John Jr., I. Samuel, M. Patrick, W. Isiah, and L. Guoqiang. 2022. "A Thermoset Shape Memory Polymer-Based Syntactic Foam with Flame Retardancy and 3D Printability." *ACS Applied Polymer Materials* 4 (2): 1183–1195. https://doi.org/10.1021/acsapm.1c01596.

Alkhasawneh, M. S., and L. Tien Tay. 2018. "A Hybrid Intelligent System Integrating the Cascade Forward Neural Network with Elman Neural Network." *Arabian Journal for Science and Engineering* 43 (12): 6737–6749. https://doi.org/10.1007/s13369-017-2833-3.

Arevo. 2022. "Making the World Lighter." https://arevo.com/.

Asif, M., J. Hyun Lee, M. J. Lin-Yip, S. Chiang, A. Levaslot, T. Giffney, M. Ramezani, and A. Kean Chin. 2018. "A New Photopolymer Extrusion 5-Axis 3D Printer." *Additive Manufacturing* 23:355–361. https://doi.org/10.1016/j.addma.2018.08.026.

Asif, M., M. Ramezani, K. Ahmed Khan, M. A. Khan, and A. Kean Chin. 2019. "Experimental and Numerical Study of the Effect of Silica Filler on the Tensile Strength of a 3D-Printed Particulate Nanocomposite." *Comptes Rendus Mécanique* 347 (9): 615–625. https://doi.org/10.1016/j.crme.2019.07.003.

Banadaki, Y., N. Razaviarab, H. Fekrmandi, L. Guoqiang, P. Mensah, S. Bai, and S. Sharifi. 2022. "Automated Quality and Process Control for Additive Manufacturing Using Deep Convolutional Neural Networks." *Recent Progress in Materials* 4 (1): 1–1. https://doi.org/10.21926/rpm.2201005.

Bikas, H., P. Stavropoulos, and G. Chryssolouris. 2016. "Additive Manufacturing Methods and Modelling Approaches: A Critical Review." *The International Journal of Advanced Manufacturing Technology* 83 (1–4): 389–405. https://doi.org/10.1007/s00170-015-7576-2.

Bin Ishak, I., J. Fisher, and P. Larochelle. 2016. "Robot Arm Platform for Additive Manufacturing Using Multi-Plane Toolpaths." In *International Design Engineering Technical Conferences and Computers and Information in Engineering Conference*, Florida, Vol. 50152, V05AT07A063. American Society of Mechanical Engineers.

Carlucho, I., D. W. Stephens, and C. Barbalata. 2021. "An Adaptive Data-Driven Controller for Underwater Manipulators with Variable Payload." *Applied Ocean Research* 113:102726. https://doi.org/10.1016/j.apor.2021.102726.

Chen, K., X. Kuang, L. Vincent, G. Kang, and H. Jerry Qi. 2018. "Fabrication of Tough Epoxy with Shape Memory Effects by UV-Assisted Direct-Ink Write Printing." *Soft Matter* 14 (10): 1879–1886. https://doi.org/10.1039/C7SM02362F.

Chen, R., P. Rao, L. Yan, E. W. Reutzel, and H. Yang. 2021. "Recurrence Network Analysis of Design-Quality Interactions in Additive Manufacturing." *Additive Manufacturing* 39:101861. https://doi.org/10.1016/j.addma.2021.101861.

Continuous Composites. 2022. "Continuous Fiber 3D Printing." https://www.continuouscomposites.com/.

Costa, M. A., B. Wullt, M. Norrlöf, and S. Gunnarsson. 2019. "Failure Detection in Robotic Arms Using Statistical Modeling, Machine Learning and Hybrid Gradient Boosting." *Measurement* 146:425–436. https://doi.org/10.1016/j.measurement.2019.06.039.

Delda, R. N. M., R. Balisalisa Basuel, R. Peralta Hacla, D. William Carpiano Martinez, J.-J. Cabibihan, and J. Ryan Cortez Dizon. 2021. "3D Printing Polymeric Materials for Robots with

Embedded Systems." *Technologies* 9 (4): 82. https://doi.org/10.3390/technologies9040082.

Delli, U., and S. Chang. 2018. "Automated Process Monitoring in 3D Printing Using Supervised Machine Learning." *Procedia Manufacturing, 46th SME North American Manufacturing Research Conference, NAMRC 46* 26: 865–870. Texas, USA, https://www.sciencedirect.com/science/article/pii/S2351978918307820 .

Deng, K., C. Zhang, and F. Kun Kelvin. 2023. "Additive Manufacturing of Continuously Reinforced Thermally Curable Thermoset Composites with Rapid Interlayer Curing." *Composites Part B Engineering* 257:110671. https://doi.org/10.1016/j.compositesb.2023.110671.

Dharmawan, A. G., Y. Xiong, S. Foong, and G. Song Soh. 2020. "A Model-Based Reinforcement Learning and Correction Framework for Process Control of Robotic Wire Arc Additive Manufacturing." In *2020 IEEE International Conference on Robotics and Automation (ICRA)*, 4030–4036. IEEE.

El Moumen, A., M. Tarfaoui, and K. Lafdi. 2019. "Additive Manufacturing of Polymer Composites: Processing and Modeling Approaches." *Composites Part B Engineering* 171:166–182. https://doi.org/10.1016/j.compositesb.2019.04.029.

Farahani, R. D., L. Laberge Lebel, and D. Therriault. 2014. "Processing Parameters Investigation for the Fabrication of Self-Supported and Freeform Polymeric Microstructures Using Ultraviolet-Assisted Three-Dimensional Printing." *Journal of Micromechanics and Microengineering* 24 (5): 055020. https://doi.org/10.1088/0960-1317/24/5/055020.

Gao, C., J. Qiu, and S. Wang. 2022. "In-Situ Curing of 3D Printed Freestanding Thermosets." *Journal of Advanced Manufacturing and Processing* 4 (3): e10114. https://doi.org/10.1002/amp2.10114.

Garfo, S., M. A. Muktadir, and Y. Sun. 2020. "Defect Detection on 3D Print Products and in Concrete Structures Using Image Processing and Convolution Neural Network." *Journal of Mechatronics and Robotics* 4 (1): 74–84. https://doi.org/10.3844/jmrsp.2020.74.84.

Gholamy, A., V. Kreinovich, and O. Kosheleva. 2018. *Why 70/30 or 80/20 Relation Between Training and Testing Sets: A Pedagogical Explanation*. UTEP-CS-18-09. Texas: The University of Texas at El Paso.

He, X., Y. Ding, Z. Lei, S. Welch, W. Zhang, M. Dunn, and Y. Kai. 2021. "3D Printing of Continuous Fiber-Reinforced Thermoset Composites." *Additive Manufacturing* 40:101921. https://doi.org/10.1016/j.addma.2021.101921.

Hershey, C., J. Lindahl, S. Romberg, A. Roschli, B. Hedger, M. Kastura, B. Compton, and V. Kunc. 2019. *Large-Scale Reactive Extrusion Deposition of Sparse Infill Structures with Solid Perimeters*. Technical Report. Oak Ridge National Lab. (ORNL), Oak Ridge, TN (United States).

Jiang, J., S. T. Newman, and R. Y. Zhong. 2021. "A Review of Multiple Degrees of Freedom for Additive Manufacturing Machines." *International Journal of Computer Integrated Manufacturing* 34 (2): 195–211. https://doi.org/10.1080/0951192X.2020.1858510.

Kopatz, J. W., J. Unangst, A. W. Cook, and L. N. Appelhans. 2021. "Compositional Effects on Cure Kinetics, Mechanical Properties and Printability of Dual-Cure Epoxy/Acrylate Resins for DIW Additive Manufacturing." *Additive Manufacturing* 46:102159. https://doi.org/10.1016/j.addma.2021.102159.

Li, A., A. Challapalli, and L. Guoqiang. 2019. "4D Printing of Recyclable Lightweight Architectures Using High Recovery Stress Shape Memory Polymer." *Scientific Reports* 9 (1): 1–13. https://doi.org/10.1038/s41598-019-44110-9.

Luu, Q. K., and L. Hung Manh. 2021. "A 3-Dimensional Printing System Using an Industrial Robotic Arm." In *2021 IEEE/SICE International Symposium on System Integration (SII)* 443–448. Japan. IEEE.

Miri, S., J. Kalman, J.-P. Canart, J. Spangler, and K. Fayazbakhsh. 2022. "Tensile and Thermal Properties of Low-Melt Poly Aryl Ether Ketone Reinforced with Continuous Carbon Fiber Manufactured by Robotic 3D Printing." *The International Journal of Advanced Manufacturing Technology* 122 (2): 1041–1053. https://doi.org/10.1007/s00170-022-09983-7.

Mitchell, T. M. 1997. *Machine Learning*. McGraw-Hill Science/Engineering/Math.

Mizuno, Y., N. Pardivala, and B. L. Tai. 2018. "Projected UV-Resin Curing for Self-Supported 3D Printing." *Manufacturing Letters* 18:24–26. https://doi.org/10.1016/j.mfglet.2018.09.005.

Mohammadi, M.-R., A. Hemmati-Sarapardeh, M. Schaffie, M. M. Husein, and M. Ranjbar. 2021. "Application of Cascade Forward Neural Network and Group Method of Data Handling to Modeling Crude Oil Pyrolysis During Thermal Enhanced Oil Recovery." *Journal of Petroleum Science and Engineering* 205:108836. https://doi.org/10.1016/j.petrol.2021.108836.

Moi Composites. 2022. "Composites Production Made Simple." https://www.moi.am/.

Nicholas, P., G. Rossi, E. Williams, M. Bennett, and T. Schork. 2020. "Integrating Real-Time Multi-Resolution Scanning and Machine Learning for Conformal Robotic 3D Printing in Architecture." *International Journal of Architectural Computing* 18 (4): 371–384. https://doi.org/10.1177/1478077120948203.

Nycz, A., Y. Lee, M. Noakes, D. Ankit, C. Masuo, S. Simunovic, J. Bunn, L. Love, V. Oancea, A. Payzant, C. M. Fancher, et al. 2021. "Effective Residual Stress Prediction Validated with Neutron Diffraction Method for Metal Large-Scale Additive Manufacturing." *Materials & Design* 205:109751. https://doi.org/10.1016/j.matdes.2021.109751.

Park, S., W. Shou, L. Makatura, W. Matusik, and F. Kun Kelvin. 2022. "3D Printing of Polymer Composites: Materials, Processes, and Applications." *Matter* 5 (1): 43–76. https://doi.org/10.1016/j.matt.2021.10.018.

Romberg, S. K., M. A. Islam, C. J. Hershey, M. DeVinney, C. E. Duty, V. Kunc, and B. G. Compton. 2021. "Linking Thermoset Ink Rheology to the Stability of 3D-Printed Structures." *Additive Manufacturing* 37:101621. https://doi.org/10.1016/j.addma.2020.101621.

Shembekar, A. V., Y. Jung Yoon, A. Kanyuck, and S. K. Gupta. 2019. "Generating Robot Trajectories for Conformal Three-Dimensional Printing Using Nonplanar Layers."

Journal of Computing and Information Science in Engineering 19 (3): 3. https://doi.org/10.1115/1.4043013.

Slic3r. 2022. "Slic3r - Open Source 3D Printing Toolbox." https://slic3r.org/ .

Tiryaki, M. E., X. Zhang, and Q.-C. Pham. 2019a. "Printing-While-Moving: A New Paradigm for Large-Scale Robotic 3D Printing." In *2019 IEEE/RSJ International Conference on Intelligent Robots and Systems (IROS)* Macau, 2286–2291.

Tiryaki, M. E., X. Zhang, and Q.-C. Pham. 2019b. "Printing-While-Moving: A New Paradigm for Large-Scale Robotic 3D Printing." In *2019 IEEE/RSJ International Conference on Intelligent Robots and Systems (IROS)* Macau, 2286–2291. IEEE.

Tu, R., and H. A. Sodano. 2021. "Additive Manufacturing of High-Performance Vinyl Ester Resin via Direct Ink Writing with UV-Thermal Dual Curing." *Additive Manufacturing* 46:102180. https://doi.org/10.1016/j.addma.2021.102180.

Tyler, K. 2014. "Method and Apparatus for Continuous Composite Three-Dimensional Printing." US Patent 2014/0061974 A1, https://patents.google.com/patent/US20140061974A1/en.

Uitz, O., P. Koirala, M. Tehrani, and C. Conner Seepersad. 2021. "Fast, Low-Energy Additive Manufacturing of Isotropic Parts via Reactive Extrusion." *Additive Manufacturing* 41:101919. https://doi.org/10.1016/j.addma.2021.101919.

Urhal, P., A. Weightman, C. Diver, and P. Bartolo. 2019. "Robot Assisted Additive Manufacturing: A Review." *Robotics and Computer-Integrated Manufacturing* 59:335–345. https://doi.org/10.1016/j.rcim.2019.05.005.

Velazquez, L., G. Palardy, and C. Barbalata. 2021. "Design and Integration of End-Effector Extruder for 3D Printing Novel UV-Curable Shape Memory Polymers with a Collaborative Robotic System. *The Composites and Advanced Materials Expo* Dallas, TX.

Wang, B., K. F. Arias, Z. Zhang, Y. Liu, Z. Jiang, H.-J. Sue, N. Currie-Gregg, S. Bouslog, Z. (J.) Pei, and S. Wang. 2019. "3D Printing of in-Situ Curing Thermally Insulated Thermosets." *Manufacturing Letters* 21:1–6. https://doi.org/10.1016/j.mfglet.2019.06.001.

Wang, B., Z. Zhang, Z. Pei, J. Qiu, and S. Wang. 2020. "Current Progress on the 3D Printing of Thermosets." *Advanced Composites and Hybrid Materials* 3 (4): 462–472. https://doi.org/10.1007/s42114-020-00183-z.

Weger, L., L. Velazquez, C. Barbalata, D. Roy, and G. Palardy. 2022. "Curing Behavior Simulator for Robotic 3D Printing of UV-Curable Thermoset Polymers." In *2022 SPE Annual Technical Conference (ANTEC)*, SPE, Charlotte, NC.

Westbeek, S., J. J. Remmers, J. A. W. Van Dommelen, and M. G. Geers. 2020. "Multi-Scale Process Simulation for Additive Manufacturing Through Particle Filled Vat Photopolymerization." *Computational Materials Science* 180:109647. https://doi.org/10.1016/j.commatsci.2020.109647.

White, F. M. 2011. Fluid Mechanics. *McGraw-Hill Series in Mechanical Engineering*. McGraw Hill. https://books.google.com/books?id=egk8SQAACAAJ.

Wu, C., C. Dai, G. Fang, Y.-J. Liu, and C. C. Wang. 2017. "RoboFdm: A Robotic System for Support-Free Fabrication Using FDM." In *2017 IEEE International Conference on Robotics and Automation (ICRA)* 1175–1180. Marina Bay Sands Singapore IEEE.

Wu, T., P. Jiang, X. Zhang, Y. Guo, J. Zhongying, X. Jia, X. Wang, F. Zhou, and W. Liu. 2019. "Additively Manufacturing High-Performance Bismaleimide Architectures with Ultraviolet-Assisted Direct Ink Writing." *Materials & Design* 180:107947. https://doi.org/10.1016/j.matdes.2019.107947.

Xiong, J., G. Zhang, H. Jianwen, and W. Lin. 2014. "Bead Geometry Prediction for Robotic GMAW-Based Rapid Manufacturing Through a Neural Network and a Second-Order Regression Analysis." *Journal of Intelligent Manufacturing* 25 (1): 157–163. https://doi.org/10.1007/s10845-012-0682-1.

Yan, C., X. Feng, and L. Guoqiang. 2021. "From Drug Molecules to Thermoset Shape Memory Polymers: A Machine Learning Approach." *ACS Applied Materials & Interfaces* 13 (50): 60508–60521. https://doi.org/10.1021/acsami.1c20947.

Yan, C., X. Feng, C. Wick, A. Peters, and L. Guoqiang. 2021. "Machine Learning Assisted Discovery of New Thermoset Shape Memory Polymers Based on a Small Training Dataset." *Polymer* 214:123351. https://doi.org/10.1016/j.polymer.2020.123351.

Zhang, J., P. Wang, and R. X. Gao. 2020. "Attention Mechanism-Incorporated Deep Learning for AM Part Quality Prediction." *Procedia CIRP* 93:96–101. https://doi.org/10.1016/j.procir.2020.04.051.

Zhang, X., L. Mingyang, J. Hui Lim, Y. Weng, Y. Wei Daniel Tay, H. Pham, and Q.-C. Pham. 2018. "Large-Scale 3D Printing by a Team of Mobile Robots." *Automation in Construction* 95:98–106. https://doi.org/10.1016/j.autcon.2018.08.004.

Ziaee, M., J. W. Johnson, and M. Yourdkhani. 2022. "3D Printing of Short-Carbon-Fiber-Reinforced Thermoset Polymer Composites via Frontal Polymerization." *ACS Applied Materials & Interfaces* 14 (14): 16694–16702. PMID: 35353492. https://doi.org/10.1021/acsami.2c02076.

Zohdi, T. I. 3. 7. 6. 1. 0. 0. 3. 2018. "Dynamic Thermomechanical Modeling and Simulation of the Design of Rapid Free-Form 3D Printing Processes with Evolutionary Machine Learning." *Computer Methods in Applied Mechanics and Engineering* 331:343–362. https://doi.org/10.1016/j.cma.2017.11.030.